Research Square

Preprints are preliminary reports that have not undergone peer review.
They should not be considered conclusive, used to inform clinical practice,
or referenced by the media as validated information.

Insights into the Stereochemistry of the Abasic Product in Thymine DNA Glycosylase: A Displacement Reaction Pathway from Computational Simulations

Wenwen Diao
Oujiang Laboratory (Zhejiang Lab for Regenerative Medicine, Vision and Brain Health), Wenzhou Institute, University of Chinese Acad-emy of Sciences

Xiaodi Fu
Faculty of Arts and Sciences, Beijing Normal University

Yuzhuo Yang
Faculty of Arts and Sciences, Beijing Normal University

Jing Peng
Faculty of Arts and Sciences, Beijing Normal University

Fangfu Ye
Oujiang Laboratory (Zhejiang Lab for Regenerative Medicine, Vision and Brain Health), Wenzhou Institute, University of Chinese Acad-emy of Sciences

Zhanfeng Wang
zfwang@bnu.edu.cn

Faculty of Arts and Sciences, Beijing Normal University

Article

Keywords: Base excision repair, Thymine DNA glycosylase, Catalytic mechanism, Stereochemistry, Abasic site, QM/MM calculations, MD simulations

Posted Date: November 18th, 2026

DOI: https://doi.org/10.21203/rs.3.rs-11517001/v1

License: This work is licensed under a Creative Commons Attribution 4.0 International License.
Read Full License

Additional Declarations: No competing interests reported.

Insights into the Stereochemistry of the Abasic Product in Thymine DNA Glycosylase: A Displacement Reaction Pathway from Computational Simulations

KEYWORDS: Base excision repair • Thymine DNA glycosylase • Catalytic mechanism • Stereochemistry • Abasic site • QM/MM calculations • MD simulations

ABSTRACT: Thymine DNA glycosylase (TDG) is a unique member of the uracil DNA glycosylase (UDG) superfamily, playing critical roles in both DNA base excision repair and epigenetic regulation. Unlike canonical UDGs and most other DNA glycosylases that generate an α-anomeric abasic site, a mix of α- and β-anomeric products was observed in the high-resolution crystal structures of TDG product complex. Despite its functional biological importance, the molecular origin of this unusual stereochemical divergence has long remained unresolved. Herein, our multiscale computational results show that the canonical ring-opened aldehyde-mediated pathway, generally accepted to govern free abasic DNA α/β anomeric interconversion in solution, is difficult to occur within the TDG active site due to the absence of auxiliary catalytic water molecules. Instead, our calculations suggest a His151-mediated displacement mechanism, in which the histidine residue acts as a general base to facilitate the stereospecific α-to-β anomeric inversion. This newly-proposed mechanism rationalizes the dual-conformation flexibility of His151 and the exclusive formation of the α-anomer in the presence of acetate ions observed in high-resolution crystal structures. These findings not only resolve the longstanding TDG-specific catalytic puzzle, but also establish a general and simple structural criterion for evaluating aldehyde-mediated anomerization mechanism of abasic site.

Introduction

DNA glycosylases are central enzymes in the base excision repair (BER) pathway, which safeguards genomic integrity by detecting and excising aberrant or damaged nucleobases.[1-3] Upon identifying a lesion, these enzymes employ a base-flipping mechanism to extrude the damaged nucleotide from the DNA helix, positioning it within the active site.[4-7] Thereafter, catalytic cleavage of the N-glycosidic bond removes the target base, leaving behind an abasic site—a highly genotoxic lesion that is subsequently repaired by downstream BER factors.[8-9] Beyond their fundamental role in maintaining genetic fidelity, dysfunction of DNA glycosylases is tightly associated with human diseases,[10] especially carcinogenesis.[11-12] The pivotal biological significance of DNA repair mechanisms was internationally recognized by the 2015 Nobel Prize in Chemistry, awarded to Tomas Lindahl, Paul Modrich, and Aziz Sancar for their ground-breaking mechanistic investigations of genome maintenance pathways.[13]

Thymine DNA glycosylase (TDG) is a monofunctional glycosylase with an unusually broad substrate spectrum.[14-16] Traditionally defined as a core BER enzyme, TDG primarily excises thymine (T) from G:T mismatches—lesions arising from the hydrolytic deamination of 5-methylcytosine (mC),[17-18] a key epigenetic regulator of gene expression.[19] It also efficiently removes uracil (U) from G:U mispairs generated via spontaneous cytosine deamination.[20] Beyond canonical BER functions, TDG plays a pivotal role in active DNA demethylation by removing 5-formylcytosine (fC)[21] and

5-carboxylcytosine (caC),[22-27] oxidative derivatives of mC generated by ten-eleven translocation (TET) enzymes.[28] To date, TDG remains the only mammalian glycosylase capable of processing fC and caC, and its genetic ablation causes embryonic lethality,[29-30] highlighting its irreplaceable physiological function. Collectively, TDG operates at the intersection of genome stability and epigenetic regulation, making the atomic-level mechanistic understanding of its catalysis an essential subject of investigation.

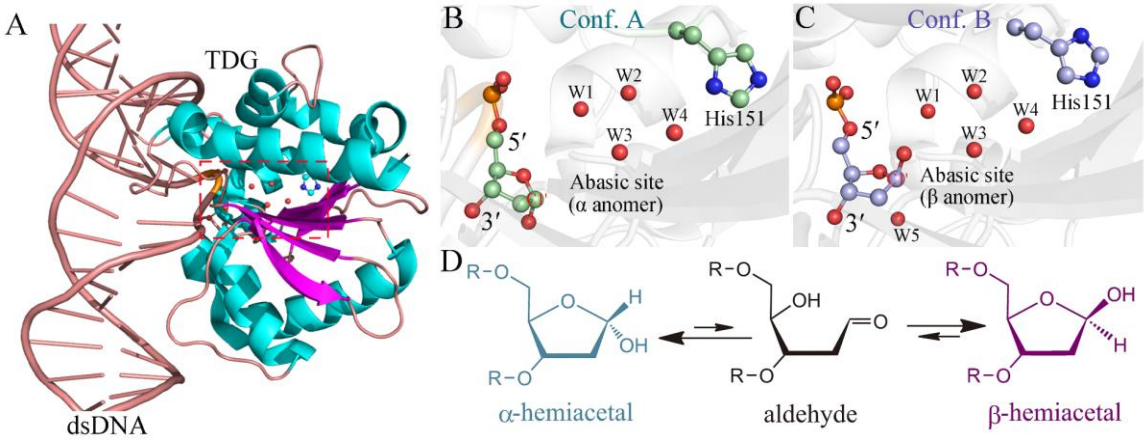


Figure 1. Crystal structure and stereochemistry of TDG abasic product. (A) The crystal structure (PDB ID: 4Z3A) of the TDG abasic product complex that contains a mix of α- and β-anomers. (B) α-anomeric abasic site. (C) β-anomeric abasic site. (D) The generally accepted anomerization mechanism via a ring-opened aldehyde intermediate.

Mechanistically, TDG has long been presumed to follow the canonical hydrolytic pathway of prototypical Uracil DNA glycosylase (UDG) enzymes,[31-33] employing a water nucleophile to excise the N-glycosidic bond between the abnormal base and the sugar-phosphate backbone. The reaction follows an S_N2 mechanism yet with a significant dissociative character, featuring an oxocarbenium-like transition state, where nucleobase departure and nucleophile addition proceed in a concerted manner.[33-37] Due to the poor nucleophilicity of water molecules, the water nucleophile is usually activated by a general base, residue Asp145 in UDG,[33, 37] that resides on the opposite side of the nucleobase (3′ side of the sugar ring), yielding an abasic site of α-anomer. Interestingly, TDG lacks such a general base, making it a special DNA glycosylase. The corresponding position in TDG is occupied by an asparagine residue (Asn140). Accordingly, the water nucleophile was found to be only partially deprotonated by a previous theoretical study.[38] The importance of this residue has been demonstrated both experimentally[39-40] and theoretically,[38, 41-43] which was suggested to anchor the attacking water nucleophile and stabilize the positive charge of the abasic site via the H-bond formed between the water nucleophile and its amide side chain.[38, 42]

High-resolution structural and nuclear magnetic resonance (NMR) studies revealed that TDG has negligible affinity for the excised base in the product complex, only water molecules and the abasic sugar observed in acetate-free conditions (refer to Figure 1).[44] Interestingly, the abasic sugar was shown to exist as a mixture of α (Figure 1B) and β (Figure 1C) anomers. However, only the α anomer was observed when acetate was present in mother liquor.[44] An updated crystal structure of TDG product complex with extended N-terminal sequences further confirmed the existence of the β anomer,[45] despite the fact that all water-dependent DNA glycosylases, including TDG, initially produce the α anomer.[1-2] It was suggested that the α-to-β conversion confers tighter binding of TDG to its abasic DNA product due to the more contacts between β anomer and TDG.[44] The anomeric conversion of abasic site is potentially coupled to the catalytic mechanism of DNA glycosylases, as exemplified by the case of adenine DNA glycosylase MutY.[37, 46-49]

It is well-established that the α/β anomeric interconversion of free DNA abasic site could transpire via a ring-opened aldehyde intermediate in aqueous situation,[50-51] as shown in Figure 1D. Accordingly, one plausible scenario is that the initially formed α anomer first dissociates from TDG, undergoes α-to-β anomeric conversion in bulk solution, and then rebinds to TDG. This mechanism could account for the β anomer observed in TDG product crystal structures. However, the absence of abasic β anomers in product crystal structures of most DNA glycosylases suggests that β-anomer formation is TDG-dependent. In addition, given the strong genotoxicity of abasic sites[8] and tight binding between TDG and abasic DNA,[52-54] the anomeric conversion most likely takes place inside the TDG active site.

Drohat and coworkers proposed that the abasic sugar undergoes dynamic α/β anomeric equilibration within the TDG active site, analogous to free abasic DNA in solution, and this equilibrium is shifted toward the α-anomer in the presence of dissociated bases or acetate buffer.[44] Alternatively, the transition may transpire via a displacement reaction, akin to the case of MutY. MutY was initially proposed to adopt a canonical hydrolysis mechanism akin to UDG, generating α-anomeric abasic site.[55-59] However, subsequent experimental[46-47, 49] and computational[48, 60] studies revised this model, establishing that MutY catalysis proceeds via a double-displacement mechanism with stereochemical retention at the C1′ anomeric carbon. Whether the aldehyde-mediated pathway is feasible within the enzyme's active site and whether a MutY-like displacement mechanism governs TDG stereoisomerization need further investigation. More importantly, elucidating the structural and environmental conditions that dictate the operative isomerization mechanism is essential to unify our understanding of stereochemical control across DNA glycosylases and broader glycoside-processing enzymes.

Although the catalytic mechanism of TDG toward different substrates, including G:T, G:fC, and G:caC mispairs, has been extensively theoretically investigated, all prior studies end with the formation of the α-anomeric abasic product.[38, 41-43] Herein, we integrate density functional theory (DFT) calculations, molecular dynamics (MD) simulations, and quantum mechanical/molecular mechanical (QM/MM) multiscale computations to systematically investigate the molecular mechanism underlying TDG-mediated α-to-β anomeric rearrangement of the abasic site. We show that the ring-opened aldehyde isomerization pathway is hard to transpire within the TDG active site, as it requires ordered auxiliary water molecules that are absent from the confined protein pocket. Instead, our results reveal a novel displacement mechanism, where a water molecule attacks the anomeric carbon from the 5′ side to drive stereochemical inversion and β-anomer generation, which aligns well with available experimental observations.

Results and Discussion

1. Aqueous aldehyde-mediated anomerization requires auxiliary water molecules. Spontaneous inter-conversion between α and β anomers of cyclic hemiacetal sugars in aqueous solution occurs via reversible ring-opening to an acyclic aldehyde intermediate, a well-established canonical pathway for abasic site anomerization.[50-51, 61] To establish a solution-phase mechanistic baseline for TDG-associated sugar isomerization, we performed systematic DFT calculations using 2-hydroxytetrahydrofuran as a minimal abasic sugar model. In the absence of explicit water molecules, ring opening toward the aldehyde intermediate proceeds across a prohibitive kinetic barrier of 29.1 kcal/mol (Figure 2A), accompanied by PT from the O1 to O2 atom (refer to TS_0 in Figure 2D and Figure S3). Notably, a significant quantum mechanical tunneling effect is identified, with an estimated barrier lowering effect of about 8.4 kcal/mol at 298.15 K. Structural analysis of TS_0 indicates that the large energetic penalty primarily arises from the strained high-energy four-membered ring formed during ring breakage (refer to Figure 2D and Figure S3).

Incorporation of one explicit catalytic water molecule markedly reduces the ring-opening barrier to 22.3 kcal/mol (Figure 2B and Figure S4), demonstrating that a single water molecule provides critical catalytic stabilization for the aldehyde-forming transition state.[62] Addition of a second water molecule yields only marginal further stabilization, with the barrier slightly decreasing to 21.1 kcal/mol (Figure 2C and Figure S5). Tunneling contributions become much smaller in these two models (< 2 kcal/mol), which can be attributed to their reduced barriers and smaller imaginary frequencies at the transition states (Figures 2E and 2F). This water-assisted catalytic trend is robust and independent of the functionals employed in calculations (Figure S6), in line with the computational results of furanose rings.[63] Taken together, our computational results reveal that the aqueous aldehyde-mediated anomerization pathway requires at least one auxiliary water molecule to achieve kinetically accessible reaction barriers, while additional water molecules offer negligible energetic benefit. This finding establishes a structural criterion for assessing aldehyde-mediated abasic site anomerization.

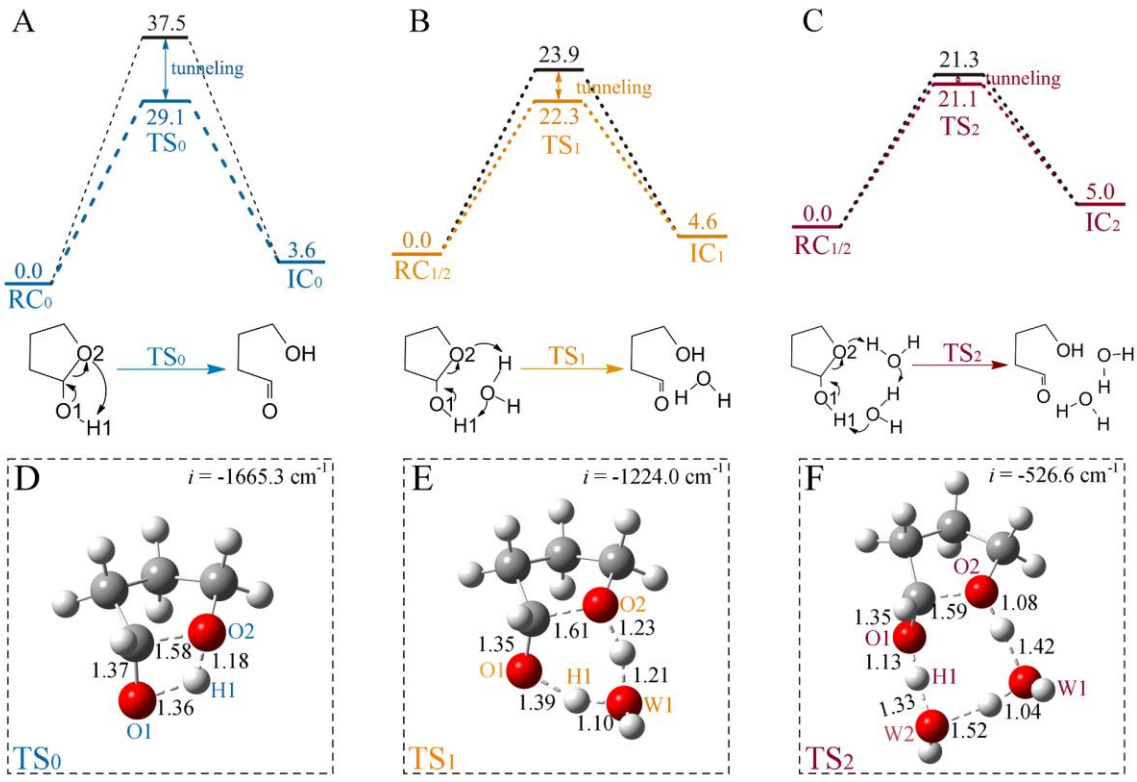


Figure 2. Aldehyde-mediated anomerization requires auxiliary water molecules. The free energy profiles (in kcal/mol) and reaction pathways of the ring-opening reaction with the assistance of 0, 1, and 2 explicit water molecules are shown in A, B, and C, respectively, while their corresponding optimized transition state geometries are shown in D, E, and F. Distances are given in Å.

2. The ring-opened aldehyde pathway is hardly accessible within the TDG active pocket. Next, we turned our attention to the case under protein environment. Structural inspection of the high-resolution TDG product crystal structure (PDB ID: 4Z3A; resolution: 1.72 Å)[44] shows no auxiliary water molecules that could form an H-bond with the hydroxyl group of α anomer to promote the sugar ring-opening reaction (Figure S7). We further verified this observation using all-atom MD simulations of the α-anomeric abasic site, with a total simulation time of 1200 ns. Beyond the well-documented strong H-bonding interaction between the α anomer and the amide side chain of Asn140 (Figures S8 and S9),[38, 41-43] a persistent H-bond is maintained between the α anomer and the backbone carbonyl oxygen of residue Thr197 (Figures S10 and S11). The binding strengths of these two H-bonds are estimated to exceed 14.7 kcal/mol (see Table

S2), confirming their nature as strong H-bonds.[64] Accordingly, water-assisted aldehyde-mediated pathways depicted in Figures 2E and 2F lack structural basis and will not be considered further.

The ring-opening reaction depicted in Figure 2D is further investigated with QM/MM method under protein environment. The computed barrier reaches 27.2 kcal/mol, with a quantum mechanical tunneling effect of 5.7 kcal/mol at 300 K (Figure 3A). Notably, prior to ring opening, the water molecule that covalently bonds with the anomeric carbon in the α anomer is only partially deprotonated (RC_A species in Figure 3). This structural feature aligns with an earlier computational characterization of the canonical 3′ water-attack pathway in TDG[38] and matches the refinement of high-resolution TDG product crystal structures.[44] This uncommon abasic site is stabilized by the strong H-bond to the amide side chain of residue Asn140, and it converts to the canonical abasic site by a feasible PT to the amide side chain of Asn140 with an energy penalty of ~2 kcal/mol.[38] The optimized geometry of the ring-opening transition state (TS_A in Figure 3) closely resembles the characterized TS structure in our solution-phase DFT calculations (TS_0 in Figure 2), featuring a strained high-energy four-membered ring. Notably, the H-bond between α anomer and Thr197 has been disrupted at TS_A, which contributes to the elevation of the energy barrier. In the resulting acyclic aldehyde intermediate (IC_A in Figure 3), a new H-bond is established between the nascent hydroxyl group and the backbone carbonyl group of residue Pro198 (refer to Figure 3D), which partially stabilizes this high-energy open-chain species. It is worth noting that the barrier height of 27.2 kcal/mol is close to the value of 29.1 kcal/mol presented in Figure 2A, representing a high activation barrier for enzymes that hardly allows the aldehyde-mediated anomeric interconversion to occur within the TDG active site under physiological conditions.

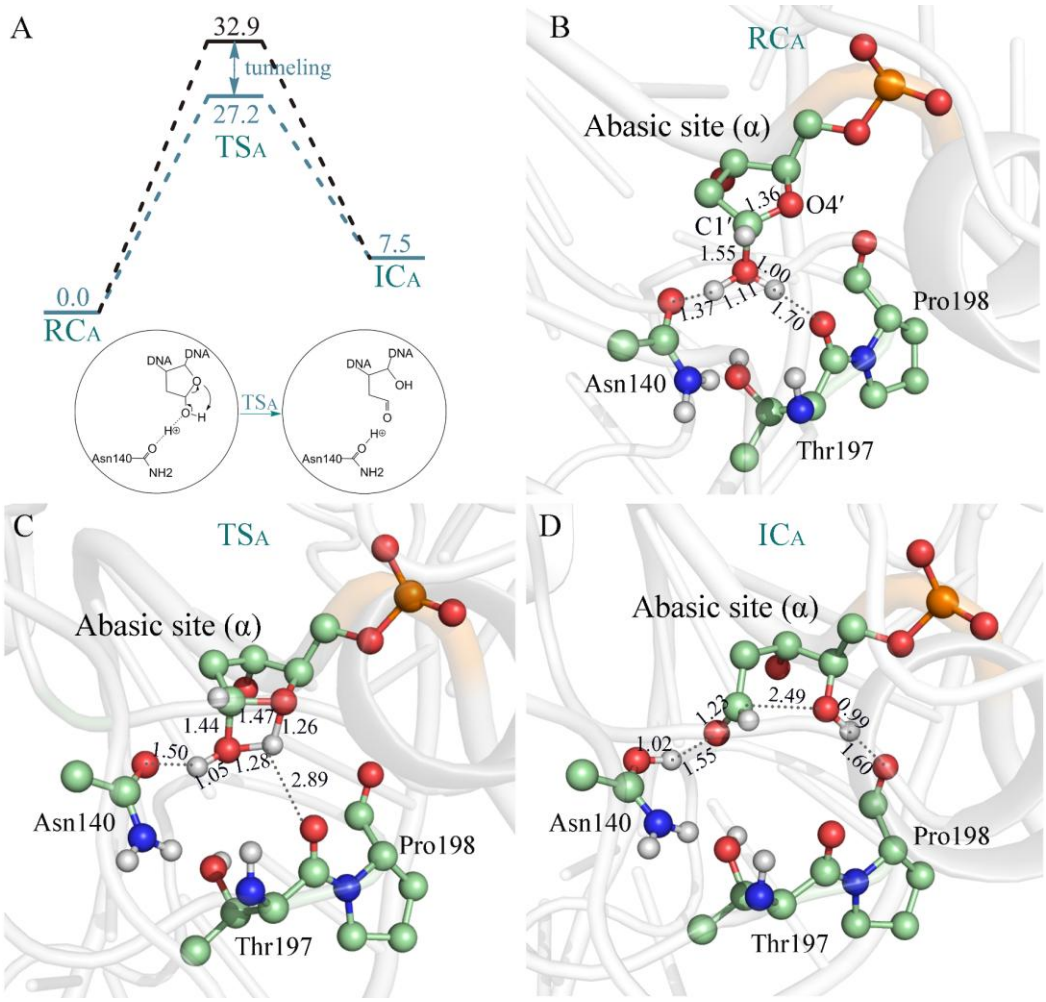


Figure 3. The aldehyde-mediated anomerization pathway is kinetically inaccessible within the TDG active pocket. (A) QM/MM calculated energy profile (in kcal/mol) of the ring-opening reaction within the TDG active pocket. QM/MM optimized geometries of the reactant complex (RC_A), transition state (TS_A), and the ring-opened aldehyde intermediate (IC_A) are shown in B, C, and D, respectively. Distances are given in Å.

3. A 5′-side water displacement reaction is possible to drive α-to-β anomeric interconversion. Drawing mechanistic inspiration from prior investigations of the monofunctional DNA glycosylase MutY,[46-49, 60] we next explored an alternative displacement pathway for abasic sugar isomerization. In this mechanism, a water nucleophile attacks the anomeric carbon (C1′) from the 5′ face of the deoxyribose ring, aided by a general base that accepts a proton from the attacking water to directly yield the β-anomeric abasic product.

3.1 His151 acts as the candidate general base for long-range proton transfer. MutY features two carboxylate residues positioned on opposing faces of the deoxyribose ring. The residue on the 3′ side forms a transient covalent adduct with the sugar to mediate glycosidic bond cleavage during the first displacement step, whereas the 5′-side carboxylate deprotonates an incoming water nucleophile to dissociate the newly-formed covalent bond in the second displacement reaction. Scrutinization of TDG product crystal structures reveals a key divergence from MutY: TDG lacks proximal aspartate or glutamate residues adjacent to C1′ capable of activating water via deprotonation. Instead, His151 constitutes the sole viable general base candidate, positioned about 10 Å from the anomeric carbon. While this distance is too large

for direct PT, the continuous solvent channel within the active pocket, which is already present in the crystal structure (refer to Figure 1B), could in principle mediate a long-range PT.

To function as a proton acceptor, His151 must adopt a singly-protonated state prior to the stereochemical rearrangement. Strikingly, the TDG crystal structure containing mixed α/β abasic anomers (PDB ID: 4Z3A) captures two distinct conformations of His151, designated conformation A and conformation B (refer to Figures 4A and 4B, respectively). By contrast, crystal structures exclusively bearing the α-anomer (PDB IDs: 4XEG, 4Z47, 4Z7B, 4Z7Z; refer to Figure S12) only populate conformation A, indicating a direct correlation between β anomer and the B conformation of His151. In conformation A, a stable H-bond links the Nε nitrogen of His151 to the backbone carbonyl oxygen of residue Pro125. Conformation B, uniquely observed in the β-anomer-containing crystal structure, requires protonation at its Nδ position to form an H-bond with the side-chain carboxylate group of residue Asp178. These structural observations support His151 as a proton acceptor, which exists as the singly-protonated HIE tautomer (conformation A) before anomeric rearrangement, and converts to the doubly-protonated HIP state (conformation B) upon completion of the stereochemical transition. Consistent with this model, our constant pH MD simulations confirm that the HIE form dominates conformation A when solvent pH ≥ 5.5 (Figure 4C).

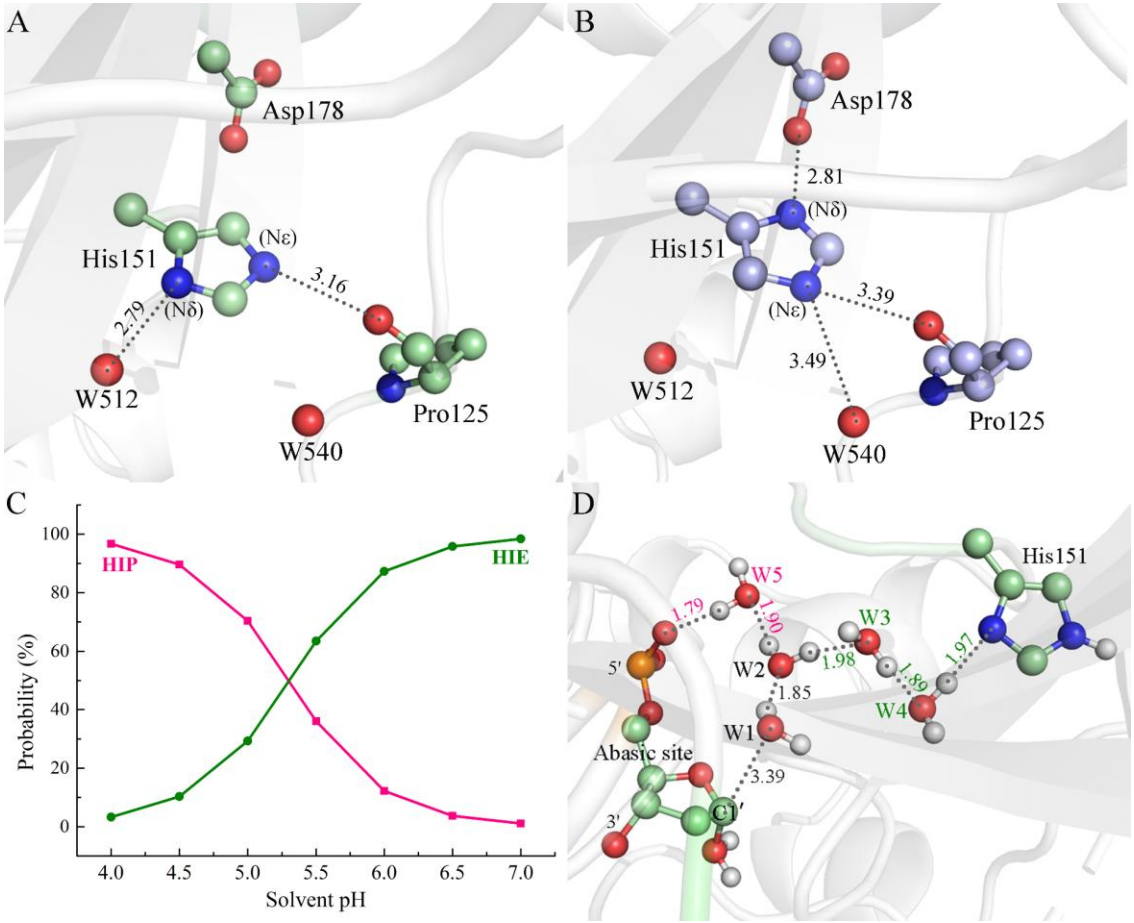


Figure 4. His151 is singly-protonated under neutral condition when the abasic site adopts an α anomer. (A) The conformation A of His151, which exists in all α-anomer-containing structures. (B) The conformation B of His151, existing only in β-anomer-containing structures. (C) Probability of different protonation forms of His151 under different solvent pH estimated with constant pH MD simulations. (D) A representative snapshot of MD simulations, where the abasic site adopts α-anomeric conformation and His151 is singly-protonated at the Nε position. The snapshot illustrates the presence of a candidate water nucleophile (labeled W1) and two long-range PT pathways. The first PT

pathway connecting W1 to the Nδ atom of His151 is composed of W2, W3, and W4, while the second PT pathway composed of W2 and W5 bridges W1 and the phosphate group of the abasic site. Distances are given in Å.

A MutY-like displacement mechanism requires two additional structural prerequisites: a nucleophilic water molecule positioned proximal to the anomeric carbon, and a continuous PT pathway linking this water nucleophile to the general base His151 to enable deprotonation. Starting from the high-resolution crystal structure (PDB ID: 4Z3A), where only the α-anomer was retained and residue His151 was locked in its HIE state, six independent 200 ns MD simulations were performed to sample the water configuration around the abasic site. Consistent with our structural hypothesis, water-bridged PT chains linking the candidate nucleophilic water and singly-protonated His151 are repeatedly sampled across MD trajectories. While these 3-4 water-bridged PT channels are dynamically labile, the rigid surrounding protein scaffold stabilizes their assembly (Figure S13). In a representative snapshot (Figure 4D), the distance between the candidate water nucleophile (labeled W1) and the C1′ anomeric carbon measures only 3.39 Å. Moreover, a continuous PT conduit composed of three intervening water molecules (W2, W3, and W4) connects W1 to the Nδ atom of His151. Collectively, our MD simulations validate the structural plausibility of this displacement pathway, prompting us to further quantify its kinetic and thermodynamic feasibility with QM/MM method.

Intriguingly, another PT route was also identified, bridging W1 to the backbone phosphate of the abasic lesion via two intermediate water molecules (W2 and W5 in Figure 4D). This observation suggests the phosphate group could potentially serve as a proton acceptor to mediate the displacement reaction, which also warrants further computational validation.

3.2 The His151-mediated displacement pathway is kinetically and thermodynamically favorable. We next performed QM/MM calculations to quantitatively assess the feasibility of the hypothesized 5′-face displacement mechanism. Three catalytically competent MD snapshots were selected as input structures for QM/MM calculations, filtered by two structural criteria: (1) the candidate nucleophilic water lies within 3.5 Å of the anomeric carbon; (2) a continuous PT channel connects this water nucleophile to His151 to facilitate water deprotonation. Across all tested conformations, the His151-assisted displacement pathway is both kinetically and thermodynamically accessible, with an average activation barrier of 14.1 ± 2.6 kcal/mol (Table S3). The overall reaction is weakly exothermic, with an average reaction energy of -4.8 ± 2.0 kcal/mol (Table S4). In stark contrast, the phosphate-mediated displacement reaction is found to be thermodynamically disfavoured, exhibiting an unfavourable reaction energy of about 13.1 kcal/mol (Figure S14). Additionally, its activation barrier is ~10 kcal/mol higher than that of the His151-dependent route, disfavoring the phosphate-mediated pathway as a viable route for anomerization. Comparison with the aldehyde-mediated pathway (Figure 3) reveals that the newly-proposed His151-mediated displacement pathway is strongly favoured and represents the most plausible mechanism.

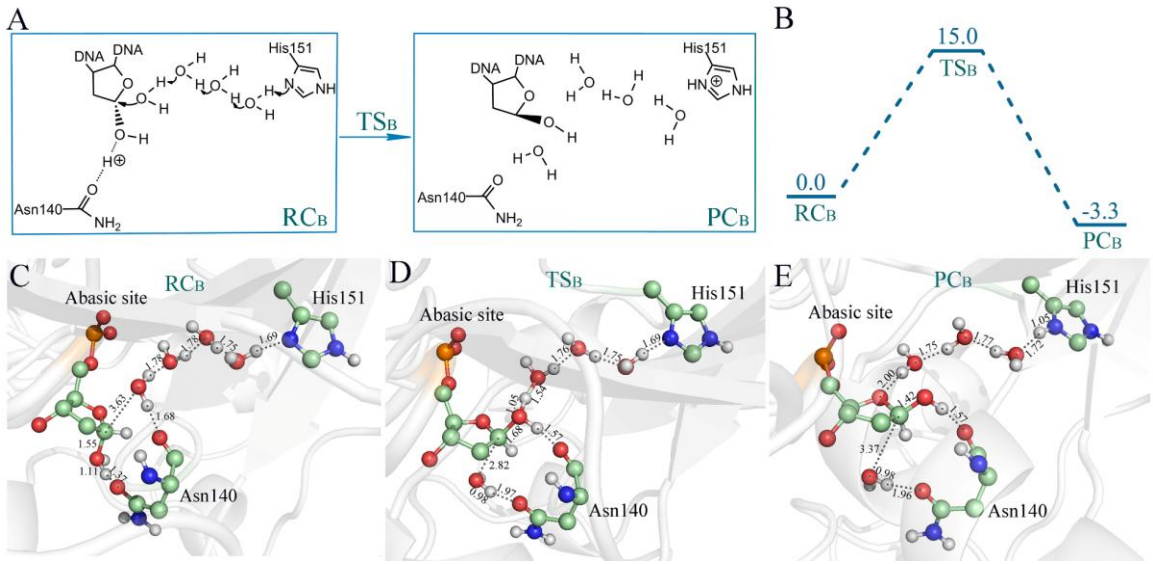


Figure 5. The His151-mediated displacement pathway is kinetically and thermodynamically feasible. (A) Schematic diagram of the reaction process. (B) QM/MM calculated energy profile (in kcal/mol) of the His151-mediated displacement reaction. QM/MM optimized geometries of the reactant complex (RC_B), transition state (TS_B), and the β-anomeric product complex (PC_B) are shown in C, D, and E, respectively. Distances are given in Å.

For direct comparison with the aldehyde-mediated pathway shown in Figure 3, the energy profile of the His151-facilitated displacement reaction calculated with the same snapshot is provided in Figure 5, while results of the other two snapshots are shown in Figures S15 and S16. At the transition state, a nearly complete covalent bond (1.68 Å) develops between the C1′ carbon and the oxygen atom of the attacking nucleophilic water, whereas proton transfer to the general base His151 remains at an incipient stage (Figure 5D). The reaction terminates with dissociation of the original 3′-side water from the deoxyribose, generating a canonical β-anomeric abasic site bearing a hydroxide moiety at the C1′ position upon completion of the PT to His151 (Figure 5E). The resulting β-anomeric product is stabilized by an H-bond between the abasic hydroxyl group and the backbone carbonyl group of Asn140. It is worth noting that the protonation state of residue His151 has changed from HIE to HIP upon the reaction completion, explaining the presence of conformation B of His151 in the crystal structures containing the β anomer. Remarkably, the activation barrier difference between our newly-uncovered His151-assisted displacement pathway (Figure 5B) and the canonical ring-opened aldehyde mechanism (Figure 3A) reaches up to ~12 kcal/mol for the same snapshot. This substantial energetic disparity provides a more direct evidence that α-to-β anomeric rearrangement of the TDG-bound abasic site proceeds predominantly through the His151-assisted 5′-water displacement mechanism. This finding corrects the long-standing oversimplified presumption that aqueous sugar isomerization mechanism can be extrapolated to enzymatic catalysis.

3.3 Structural basis for the suppressed β-anomer formation in acetate-containing buffer. Experimental studies have shown that the β-anomeric abasic species is detected only under acetate-free conditions.[44] Our classical MD simulations provide a structural rationale for this acetate-sensitive stereochemistry. Bound acetate exhibits high conformational stability within the active pocket, with an average RMSD value of merely 0.6 Å across 400 ns MD simulations (Figure 6A; Figure S17). Its carboxylate carbon remains ~4.7 Å away from the C1′ anomeric carbon throughout the simulation (Figure S18). As illustrated in Figure 6B, acetate is rigidly anchored via an extensive hydrogen-bond network formed by the backbones of Ile139 and Asn230, the side chains of Asn157 and Ser271, and two ordered solvent waters. The acetate ion stably occupies the 5′ face of the deoxyribose ring, sterically occluding solvent access to the anomeric center.

Collectively, tightly bound acetate physically blocks nucleophilic water molecules from approaching the 5′ face of the sugar scaffold, inhibiting the His151-assisted displacement pathway that is proposed to drive α-to-β anomeric conversion of the abasic site.

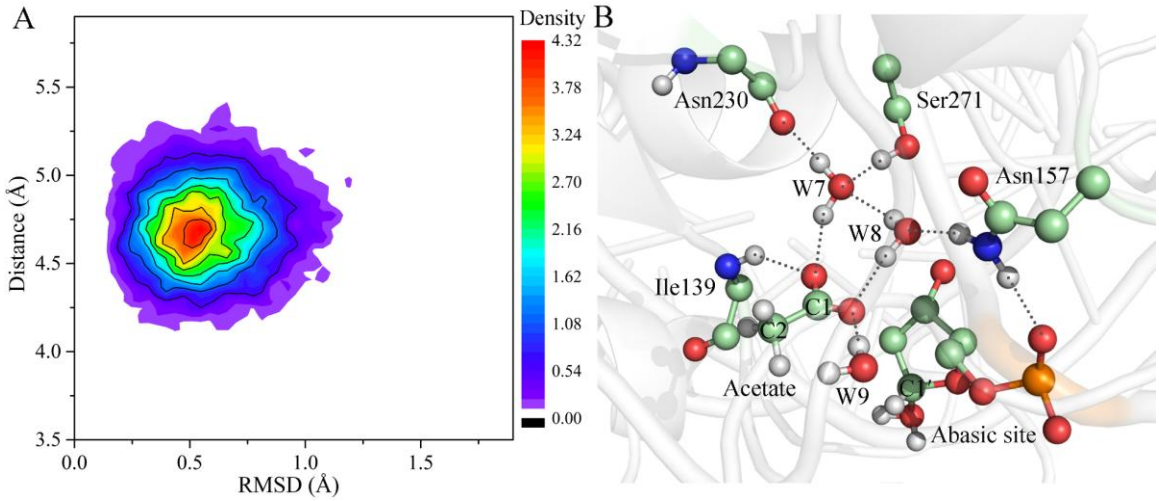


Figure 6. Acetate stably occupies the 5′ face of the deoxyribose ring. (A) Two-dimensional (2D) density map that qualitatively show the distribution of the RMSD values of acetate and the distance between C1′ anomeric carbon and the C1 atom of acetate along MD simulations. (B) A representative snapshot of MD simulations, illustrating the hydrogen bonds formed around the acetate ion.

Conclusion

In summary, the molecular mechanism governing α-to-β stereochemical conversion of abasic sites within TDG active pocket is computationally investigated in detail. Our solution-phase DFT calculations show that the widely recognized ring-opened aldehyde mutarotation pathway demands at least one auxiliary water molecule to achieve viable reaction barriers. This canonical solvent-dependent pathway, nevertheless, is hardly accessible within the TDG active pocket: a rigid hydrogen-bond network anchored by residues Asn140 and Thr197 sterically blocks access of required exogenous solvent molecules. Computational evidence instead proposes a protein-facilitated displacement reaction as the plausible anomerization pathway. In this mechanism, a water nucleophile attacks the C1′ anomeric carbon from the 5′ face of deoxyribose, while His151 serves as a general base to mediate long-range proton transfer through water-bridged channels. This newly-defined His151-dependent 5′-water displacement mechanism well explains existing experimental results regarding to the dual conformational states of His151 in crystal structures bearing mixed α/β anomers and acetate-induced suppression of β-anomer formation. Beyond resolving the longstanding TDG-specific catalytic puzzle, our findings revise the prevailing paradigm for DNA glycosylase stereocatalysis and provide atomic-level mechanistic insights into how active-site microenvironments precisely tune the stereochemical outcome of glycosidic bond cleavage.

Computational Methods

System Setup. Two distinct computational models were constructed on the basis of high-resolution TDG product crystal structures to separately characterize the α-to-β anomerization of abasic sites (system I) and acetate-induced stereo-suppression of the β anomer (system II). System I was built from a high-resolution enzyme-product complex crystal structure (PDB ID: 4Z3A; resolution: 1.72 Å) reported by Malik et al.,[44] which contains a mixture of α- and β-anomeric abasic sites. The β anomer was manually deleted, retaining only the α anomer. Notably, two discrete conformations of

His151 are observed in this structure; conformation A was adopted in the model construction, consistent with crystallographic data showing exclusive population of conformation A in all α-anomer-only TDG product structures. System II was prepared based on a second enzyme-product complex (PDB ID: 4Z47; resolution: 1.45 Å),[44] which captures a sole α-anomeric abasic site with an acetate ion bound to the 5' face of the abasic site sugar ring. All crystal water molecules were retained. The Amber ff14SB force field was employed for normal protein residues and nucleotides.[65] Parameters for the acetate ion were generated using the general AMBER force field (GAFF),[66] with partial atomic charges derived from the RESP method[67] at the HF/6-31G(d) level of theory. For the special water-bound α-anomeric abasic site, we modelled it as a water-bound oxocarbenium species: we adopted the standard Amber atom types, while the partial atom charges were refit with the RESP method. Missing parameters were complemented using the parmchk2 utility from AmberTools. The protonation states of titratable residues (histidine, glutamate, and aspartate) were assigned on the basis of the pKa values from the PROPKA software[68] in combination with careful visual inspection of local hydrogen-bond networks. Histidine residues 151, 158, 175, 257, and 287 were singly protonated at the ε position (HIE); Histidine residues 150 and 179 were doubly protonated at both the δ and ε positions (HIP). With the exception of residue Glu236, all glutamate and aspartate were deprotonated. The resulting systems were then solvated in a rectangular box of TIP3P[69] waters extending up to at least a minimum cutoff of 12 Å from the protein surface. Finally, sodium ions (Na^+) were added to make our systems electrically neutral.

MD Simulations. Systems I and II were energy minimized using a combination of the steepest descent and conjugate-gradient methods for the solvent molecules first and then for the whole system. Subsequently, the system was gently heated from 0 to 300 K in the canonical ensemble for 300 ps, using a weak restraint of 25 kcal·mol^{-1}·Å^{-2} on the non-solvent atoms. A 1 ns of density equilibration followed, employing an isothermal-isobaric Langevin thermostat[70] and a Berendsen barostat[71] at 300 K and 1.0 atm with a collision frequency of 2 ps^{-1} and a pressure relaxation time of 1 ps to achieve a uniform density. For system I, six independent 200 ns production MD simulations (1200 ns in total) were performed to do sampling. For system II, two independent 200 ns production MD simulations (400 ns in total) were conducted to validate the stability of the acetate ion. In all MD simulations, an integration step of 2 fs was used, and covalent bonds containing hydrogen were constrained by the SHAKE algorithm.[72] Nonbonded interactions were treated with the Particle Mesh Ewald method[73] with a 10 Å cutoff. All MD simulations were performed with the GPU version of the Amber 24 package.[74-75]

Constant pH MD Simulations. Explicit-solvent constant pH MD simulations employing discrete protonation states were carried out to quantify the population fractions of distinct protonation forms of residue His151 at varying pH conditions.[76-78] In this method, standard MD trajectories are propagated in explicit solvent, while protonation-state changes are attempted in implicit solvent at fixed intervals. Seven independent 100 ns constant pH MD simulations were conducted, spanning a pH range of 4.0 to 7.0 in 0.5 pH-unit increments. Protonation-state changes were attempted every 200 fs for all simulations. The solvent relaxation time was set to 300 fs as recommended by Swails et al.[76]

QM/MM Calculation. Three snapshots extracted from the MD simulation trajectories of system I were used as initial inputs for QM/MM calculations.[79-80] All QM/MM calculations were performed with ChemShell software,[81] combining Turbomole[82] for the QM region and DL_POLY[83] for the MM region. For the formation of a ring-opened aldehyde intermediate from the α-anomeric abasic site and the proposed His151-mediated displacement reaction, the QM region consists of the abasic site of α anomer, the phosphodiester groups of both its 3′ and 5′ sides, the side chains of residues Asn140, His151, Tyr152, Asn157, and Asn191, and several water molecules above the sugar ring, which include the

potential water nucleophile and water molecules that form the proton transfer (PT) channel (Figure S1). For the phosphate-mediated displacement reaction, the QM region contains the α-anomeric abasic site, the phosphodiester groups of both its 3′ and 5′ sides, the side chains of residues Asn140 and Asn157, and 3 water molecules above the sugar ring, which include the potential water nucleophile and two water molecules that form the PT channel (refer to Figure S2). The electronic embedding scheme[79] was used to account for the polarizing effect of the enzyme environment on the QM region. Hydrogen link atoms with the charge-shift model were applied to treat the QM/MM boundary. The hybrid B3LYP density functional[84-86] with two levels of theory was applied to the QM region, while the MM region was treated with the Amber parameters. B3LYP was chosen due to its good balance between accuracy and efficiency in the studies of DNA glycosylases.[38, 43, 57, 87] Transition states were located with relaxed potential energy surface scans followed by TS optimizations using the dimer optimizer implemented in the DL-FIND code. For geometry optimization and scanning calculations, a small basis set of 6-31+G(d) (labeled B1) was used. The electronic energies of all stationary and transition state species were further corrected with a larger basis set of 6-311+G(d,p) (labeled B2). Dispersion corrections computed with Grimme's D3 method[88] were included in the QM region of all QM/MM calculations. Given the significant quantum tunneling effect observed for the aldehyde-mediated pathway, we performed vibrational frequency calculations for all stationary points of it. Local minima were confirmed to have zero imaginary frequencies, while the transition state exhibited exactly one imaginary frequency, which was further utilized to quantify the quantum mechanical tunneling contribution with the Skodje-Truhlar method.[89-90] For the His151-mediated displacement reaction, we performed frequency analysis on the snapshot with the highest activation barrier (snapshot 2) to evaluate the difference between the electronic energy and free energy profiles. As shown in Table S1, the free energy correction contributed modestly to the energy profile. Therefore, the electronic energies computed at the B3LYP-D3/B2 level were treated as a reliable approximation to the free energies. This approximation scheme is widely used in previous computational studies[91-95] and is further justified by following three reasons: (1) Full frequency calculations for large QM/MM systems would impose substantial computational overhead. (2) It is well-established that energetic discrepancies between QM/MM electronic and free energy profiles are generally modest for local chemical events within enzyme active pockets.[96] (3) Prior computational studies[37, 60, 97-99] have demonstrated negligible entropic contributions to the reactions catalysed by DNA glycosylases.

QM calculations. The stationary species for the ring-opening reaction of 2-hydroxytetrahydrofuran in aqueous solution were fully optimized at the B3LYP-D3/B1 level. Local minima and transition states were verified to possess zero and only one imaginary frequency, respectively. The electronic energies were further corrected using the def2-TZVPP basis set and the functionals B3LYP-D3 and M062X-D3.[100] The implicit waters were conducted with the SMD model.[101] The Skodje-Truhlar formalism[89-90] was adopted to evaluate the quantum mechanical tunneling effect associated with aqueous ring-opening reactions. The final reported free energy profiles incorporate both the vibrational thermal corrections and the quantum mechanical tunneling corrections. All QM calculations were performed with the Gaussian 16 (G16) software.[102]

ASSOCIATED CONTENT

Supporting Information. This material is available free of charge via the Internet.

Figures S1-S18, Table S1-S15, and the cartesian coordinates of the QM region for all computed species (PDF)

Notes

The authors declare no competing financial interest.

ABBREVIATIONS

TDG, thymine DNA glycosylase; UDG, uracil DNA glycosylase; BER, base excision repair; T, thymine; mC, 5-methylcytosine; U, uracil; G, guanine; fC, 5-formylcytosine; caC, 5-carboxylcytosine; TET, ten-eleven translocation; Asn, asparagine; His, histidine; NMR, nuclear magnetic resonance; MutY, adenine DNA glycosylase; DFT, density functional theory; MD, molecular dynamics; QM/MM, quantum mechanical/molecular mechanical; MUG, mismatch-specific uracil DNA glycosylase; PT, proton transfer; RC, reactant complex; TS, transition state; IC, intermediate complex; PC, product complex; RMSD, root mean square deviation; 2D, 2-dimensional; GAFF, general AMBER force field; RESP, restrained electrostatic potential; G16, Gaussian 16.

REFERENCES

1. Stivers, J. T.; Jiang, Y. L., A mechanistic perspective on the chemistry of DNA repair glycosylases. *Chem Rev* **2003,** *103* (7), 2729-2759.
2. Berti, P. J.; McCann, J. A. B., Toward a detailed understanding of base excision repair enzymes: transition state and mechanistic analyses of N-glycoside hydrolysis and N-glycoside transfer. *Chem Rev* **2006,** *106* (2), 506-555.
3. Drohat, A. C.; Coey, C. T., Role of Base Excision "Repair" Enzymes in Erasing Epigenetic Marks from DNA. *Chem Rev* **2016,** *116* (20), 12711-12729.
4. Slupphaug, G.; Mol, C. D.; Kavli, B.; Arvai, A. S.; Krokan, H. E.; Tainer, J. A., A nucleotide-flipping mechanism from the structure of human uracil-DNA glycosylase bound to DNA. *Nature* **1996,** *384* (6604), 87-92.
5. Dow, B. J.; Malik, S. S.; Drohat, A. C., Defining the Role of Nucleotide Flipping in Enzyme Specificity Using ^{19}F NMR. *J Am Chem Soc* **2019,** *141* (12), 4952-4962.
6. Pidugu, L. S.; Gustafson, E. E.; Servius, H. W.; Cook, M. E.; Lee, N. C.; Varney, K. M.; Drohat, A. C., Observing nucleotide flipping in DNA using indirect 2′-F nucleotide probes and ^{19}F NMR. *Nucleic Acids Res* **2025,** *53* (11), gkaf492.
7. Da, L. T.; Yu, J., Base-flipping dynamics from an intrahelical to an extrahelical state exerted by thymine DNA glycosylase during DNA repair process. *Nucleic Acids Res* **2018,** *46* (11), 5410-5425.
8. Sczepanski, J. T.; Wong, R. S.; McKnight, J. N.; Bowman, G. D.; Greenberg, M. M., Rapid DNA-protein cross-linking and strand scission by an abasic site in a nucleosome core particle. *P Natl Acad Sci USA* **2010,** *107* (52), 22475-22480.
9. Schermerhorn, K. M.; Delaney, S., A Chemical and Kinetic Perspective on Base Excision Repair of DNA. *Accounts Chem Res* **2014,** *47* (4), 1238-1246.
10. Nelson, B. C.; Dizdaroglu, M., Implications of DNA damage and DNA repair on human diseases. *Mutagenesis* **2020,** *35* (1), 1-3.
11. Hoeijmakers, J. H. J., Genome maintenance mechanisms for preventing cancer. *Nature* **2001,** *411* (6835), 366-374.
12. David, S. S.; O'Shea, V. L.; Kundu, S., Base-excision repair of oxidative DNA damage. *Nature* **2007,** *447* (7147), 941-950.
13. Lindahl, T., Instability and Decay of the Primary Structure of DNA. *Nature* **1993,** *362* (6422), 709-715.
14. Bennett, M. T.; Rodgers, M. T.; Hebert, A. S.; Ruslander, L. E.; Eisele, L.; Drohat, A. C., Specificity of human thymine DNA glycosylase depends on N-glycosidic bond stability. *J Am Chem Soc* **2006,** *128* (38), 12510-12519.
15. Cortázar, D.; Kunz, C.; Saito, Y.; Steinacher, R.; Schär, P., The enigmatic thymine DNA glycosylase. *DNA Repair* **2007,** *6* (4), 489-504.
16. Servius, H. W.; Drohat, A. C., Characterizing the excision of 7,8-dihydro-8-oxoadenine by thymine DNA glycosylase. *J Biol Chem* **2025,** *301* (7), 110363.
17. Wiebauer, K.; Jiricny, J., Mismatch-Specific Thymine DNA Glycosylase and DNA Polymerase-Beta Mediate the Correction of G.T Mispairs in Nuclear Extracts from Human-Cells. *P Natl Acad Sci USA* **1990,** *87* (15), 5842-5845.
18. Neddermann, P.; Gallinari, P.; Lettieri, T.; Schmid, D.; Truong, O.; Hsuan, J. J.; Wiebauer, K.; Jiricny, J., Cloning and expression of human G/T mismatch-specific thymine-DNA glycosylase. *J Biol Chem* **1996,** *271* (22), 12767-12774.

19. Smith, Z. D.; Hetzel, S.; Meissner, A., DNA methylation in mammalian development and disease. *Nat Rev Genet* **2025,** *26* (1), 7-30.

20. Neddermann, P.; Jiricny, J., Efficient Removal of Uracil from G•U Mispairs by the Mismatch-Specific Thymine DNA Glycosylase from Hela Cells. *P Natl Acad Sci USA* **1994,** *91* (5), 1642-1646.

21. Pidugu, L. S.; Flowers, J. W.; Coey, C. T.; Pozharski, E.; Greenberg, M. M.; Drohat, A. C., Structural Basis for Excision of 5-Formylcytosine by Thymine DNA Glycosylase. *Biochemistry-Us* **2016,** *55* (45), 6205-6208.

22. Maiti, A.; Drohat, A. C., Thymine DNA Glycosylase Can Rapidly Excise 5-Formylcytosine and 5-Carboxylcytosine. *J Biol Chem* **2011,** *286* (41), 35334-35338.

23. Hashimoto, H.; Hong, S.; Bhagwat, A. S.; Zhang, X.; Cheng, X. D., Excision of 5-hydroxymethyluracil and 5-carboxylcytosine by the thymine DNA glycosylase domain: its structural basis and implications for active DNA demethylation. *Nucleic Acids Res* **2012,** *40* (20), 10203-10214.

24. Hashimoto, H.; Zhang, X.; Cheng, X. D., Selective Excision of 5-Carboxylcytosine by a Thymine DNA Glycosylase Mutant. *J Mol Biol* **2013,** *425* (6), 971-976.

25. Pidugu, L. S.; Dai, Q.; Malik, S. S.; Pozharski, E.; Drohat, A. C., Excision of 5-Carboxylcytosine by Thymine DNA Glycosylase. *J Am Chem Soc* **2019,** *141* (47), 18851-18861.

26. Swarna, L.; Pidugu, M.; Gustafson, E.; Manglani, A.; Drohat, A., Mechanistic Insights into Acid-Catalyzed Excision of 5-Carboxylcytosine by Thymine DNA Glycosylase. *J Biol Chem* **2026,** *302* (5), 112070.

27. Maiti, A.; Michelson, A. Z.; Armwood, C. J.; Lee, J. K.; Drohat, A. C., Divergent Mechanisms for Enzymatic Excision of 5-Formylcytosine and 5-Carboxylcytosine from DNA. *J Am Chem Soc* **2013,** *135* (42), 15813-15822.

28. He, Y. F.; Li, B. Z.; Li, Z.; Liu, P.; Wang, Y.; Tang, Q. Y.; Ding, J. P.; Jia, Y. Y.; Chen, Z. C.; Li, L.; Sun, Y.; Li, X. X.; Dai, Q.; Song, C. X.; Zhang, K. L.; He, C.; Xu, G. L., Tet-Mediated Formation of 5-Carboxylcytosine and Its Excision by TDG in Mammalian DNA. *Science* **2011,** *333* (6047), 1303-1307.

29. Cortázar, D.; Kunz, C.; Selfridge, J.; Lettieri, T.; Saito, Y.; MacDougall, E.; Wirz, A.; Schuermann, D.; Jacobs, A. L.; Siegrist, F.; Steinacher, R.; Jiricny, J.; Bird, A.; Schär, P., Embryonic lethal phenotype reveals a function of TDG in maintaining epigenetic stability. *Nature* **2011,** *470* (7334), 419-U210.

30. Cortellino, S.; Xu, J. F.; Sannai, M.; Moore, R.; Caretti, E.; Cigliano, A.; Le Coz, M.; Devarajan, K.; Wessels, A.; Soprano, D.; Abramowitz, L. K.; Bartolomei, M. S.; Rambow, F.; Bassi, M. R.; Bruno, T.; Fanciulli, M.; Renner, C.; Klein-Szanto, A. J.; Matsumoto, Y.; Kobi, D.; Davidson, I.; Alberti, C.; Larue, L.; Bellacosa, A., Thymine DNA Glycosylase Is Essential for Active DNA Demethylation by Linked Deamination-Base Excision Repair. *Cell* **2011,** *146* (1), 67-79.

31. Mol, C. D.; Arvai, A. S.; Slupphaug, G.; Kavli, B.; Alseth, I.; Krokan, H. E.; Tainer, J. A., Crystal-Structure and Mutational Analysis of Human Uracil-DNA Glycosylase - Structural Basis for Specificity and Catalysis. *Cell* **1995,** *80* (6), 869-878.

32. Drohat, A. C.; Jagadeesh, J.; Ferguson, E.; Stivers, J. T., Role of electrophilic and general base catalysis in the mechanism of Escherichia coli uracil DNA glycosylase. *Biochemistry-Us* **1999,** *38* (37), 11866-11875.

33. Dinner, A. R.; Blackburn, G. M.; Karplus, M., Uracil-DNA glycosylase acts by substrate autocatalysis. *Nature* **2001,** *413* (6857), 752-755.

34. Werner, R. M.; Stivers, J. T., Kinetic isotope effect studies of the reaction catalyzed by uracil DNA glycosylase: Evidence for an oxocarbenium ion-uracil anion intermediate. *Biochemistry-Us* **2000,** *39* (46), 14054-14064.

35. Przybylski, J. L.; Wetmore, S. D., A QM/QM Investigation of the hUNG2 Reaction Surface: The Untold Tale of a Catalytic Residue. *Biochemistry-Us* **2011,** *50* (19), 4218-4227.

36. Naydenova, E.; Rossbach, S.; Ochsenfeld, C., QM/MM Study of the Uracil DNA Glycosylase Reaction Mechanism: A Competition between Asp145 and His148. *J Chem Theory Comput* **2019,** *15* (8), 4344-4350.

37. Diao, W. W.; Yan, S. H.; Farrell, J. D.; Wang, B. J.; Ye, F. F.; Wang, Z. F., Preorganized Internal Electric Field Powers Catalysis in the Active Site of Uracil-DNA Glycosylase. *Acs Catal* **2022,** *12* (20), 12488-12499.

38. Diao, W. W.; Peng, J.; Fu, X. D.; Ye, F. F.; Wang, Z. F., Preorganized Internal Electric Field Enables Nucleophilic Attack of a Nonactivated Water Molecule in Thymine DNA Glycosylase. *J Am Chem Soc* **2025,** *147* (29), 25919-25930.

39. Hardeland, U.; Bentele, M.; Jiricny, J.; Schär, P., Separating substrate recognition from base hydrolysis in human thymine DNA glycosylase by mutational analysis. *J Biol Chem* **2000,** *275* (43), 33449-33456.
40. Maiti, A.; Noon, M. S.; MacKerell, A. J. r.; Pozharski, E.; Drohat, A. C., Lesion processing by a repair enzyme is severely curtailed by residues needed to prevent aberrant activity on undamaged DNA. *P Natl Acad Sci USA* **2012,** *109* (21), 8091-8096.
41. Kanaan, N.; Crehuet, R.; Imhof, P., Mechanism of the Glycosidic Bond Cleavage of Mismatched Thymine in Human Thymine DNA Glycosylase Revealed by Classical Molecular Dynamics and Quantum Mechanical/Molecular Mechanical Calculations. *J Phys Chem B* **2015,** *119* (38), 12365-12380.
42. Naydenova, E.; Dietschreit, J. C. B.; Ochsenfeld, C., Reaction Mechanism for the N-Glycosidic Bond Cleavage of 5-Formylcytosine by Thymine DNA Glycosylase. *J Phys Chem B* **2019,** *123* (19), 4173-4179.
43. Wang, W. J.; Wang, T.; Zhao, Y.; Li, B. N.; Chen, D. Z., Theoretical Insights into N-Glycoside Bond Cleavage of 5-Carboxycytosine by Thymine DNA Glycosylase: A QM/MM Study. *J Phys Chem B* **2024,** *128* (19), 4621-4630.
44. Malik, S. S.; Coey, C. T.; Varney, K. M.; Pozharski, E.; Drohat, A. C., Thymine DNA glycosylase exhibits negligible affinity for nucleobases that it removes from DNA. *Nucleic Acids Res* **2015,** *43* (19), 9541-9552.
45. Coey, C. T.; Malik, S. S.; Pidugu, L. S.; Varney, K. M.; Pozharski, E.; Drohat, A. C., Structural basis of damage recognition by thymine DNA glycosylase: Key roles for N-terminal residues. *Nucleic Acids Res* **2016,** *44* (21), 10248-10258.
46. Woods, R. D.; O'Shea, V. L.; Chu, A.; Cao, S.; Richards, J. L.; Horvath, M. P.; David, S. S., Structure and stereochemistry of the base excision repair glycosylase MutY reveal a mechanism similar to retaining glycosidases. *Nucleic Acids Res* **2016,** *44* (2), 801-810.
47. Demir, M.; Russelburg, L. P.; Lin, W. J.; Trasvina-Arenas, C. H.; Huang, B. L.; Yuen, P. K.; Horvath, M. P.; David, S. S., Structural snapshots of base excision by the cancer-associated variant MutY N146S reveal a retaining mechanism. *Nucleic Acids Res* **2023,** *51* (3), 1034-1049.
48. Nikkel, D. J.; Wetmore, S. D., Distinctive Formation of a DNA-Protein Cross-Link during the Repair of DNA Oxidative Damage: Insights into Human Disease from MD Simulations and QM/MM Calculations. *J Am Chem Soc* **2023,** *145* (24), 13114-13125.
49. Majumdar, C.; Demir, M.; Merrill, S. R.; Hashemian, M.; David, S. S., FSHing for DNA Damage: Key Features of MutY Detection of 8-Oxoguanine:Adenine Mismatches. *Accounts Chem Res* **2024,** *57* (7), 1019-1031.
50. Manoharan, M.; Ransom, S. C.; Mazumder, A.; Gerlt, J. A.; Wilde, J. A.; Withka, J. A.; Bolton, P. H., The Characterization of Abasic Sites in DNA Heteroduplexes by Site Specific Labeling with C-13. *J Am Chem Soc* **1988,** *110* (5), 1620-1622.
51. Wilde, J. A.; Bolton, P. H.; Mazumder, A.; Manoharan, M.; Gerlt, J. A., Characterization of the Equilibrating Forms of the Aldehydic Abasic Site in Duplex DNA by O-17 NMR. *J Am Chem Soc* **1989,** *111* (5), 1894-1896.
52. Waters, T. R.; Swann, P. F., Kinetics of the action of thymine DNA glycosylase. *J Biol Chem* **1998,** *273* (32), 20007-20014.
53. Waters, T. R.; Gallinari, P.; Jiricny, J.; Swann, P. F., Human thymine DNA glycosylase binds to apurinic sites in DNA but is displaced by human apurinic endonuclease 1. *J Biol Chem* **1999,** *274* (1), 67-74.
54. Morgan, M. T.; Maiti, A.; Fitzgerald, M. E.; Drohat, A. C., Stoichiometry and affinity for thymine DNA glycosylase binding to specific and nonspecific DNA. *Nucleic Acids Res* **2011,** *39* (6), 2319-2329.
55. Fromme, J. C.; Banerjee, A.; Huang, S. J.; Verdine, G. L., Structural basis for removal of adenine mispaired with 8-oxoguanine by MutY adenine DNA glycosylase. *Nature* **2004,** *427* (6975), 652-656.
56. McCann, J. A. B.; Berti, P. J., Transition-state analysis of the DNA repair enzyme MutY. *J Am Chem Soc* **2008,** *130* (17), 5789-5797.
57. Kaur, R.; Nikkel, D. J.; Wetmore, S. D., Computational studies of DNA repair: Insights into the function of monofunctional DNA glycosylases in the base excision repair pathway. *Wires Comput Mol Sci* **2020,** *10* (5), e1471.
58. Brunk, E.; Arey, J. S.; Rothlisberger, U., Role of Environment for Catalysis of the DNA Repair Enzyme MutY. *J Am Chem Soc* **2012,** *134* (20), 8608-8616.
59. Kellie, J. L.; Wilson, K. A.; Wetmore, S. D., Standard Role for a Conserved Aspartate or More Direct Involvement in Deglycosylation? An ONIOM and MD Investigation of Adenine-DNA Glycosylase. *Biochemistry-Us* **2013,** *52* (48), 8753-8765.
60. Diao, W. W.; Farrell, J. D.; Wang, B. J.; Ye, F. F.; Wang, Z. F., Preorganized Internal Electric Field Promotes a Double-Displacement Mechanism for the Adenine Excision Reaction by Adenine DNA Glycosylase. *J Phys Chem B* **2023,** *127* (40), 8551-8564.

61. Fan, C. C.; Zhan, X. L.; Guo, F. M.; Li, Q.; Lu, K.; Shan, X. J.; Zhou, Y. F.; Ren, M. T.; Greenberg, M. M.; Liu, Y. J.; Zhou, C. Z., Uridine Embedded within DNA is Repaired by Uracil DNA Glycosylase via a Mechanism Distinct from That of Ribonuclease H2. *J Am Chem Soc* **2025,** *147* (13), 11574-11583.

62. Lewis, B. E.; Choytun, N.; Schramm, V. L.; Bennett, A. J., Transition states for glucopyranose interconversion. *J Am Chem Soc* **2006,** *128* (15), 5049-5058.

63. Alkorta, I.; Popelier, P. L. A., Computational study of mutarotation in erythrose and threose. *Carbohyd Res* **2011,** *346* (18), 2933-2939.

64. Steiner, T., The hydrogen bond in the solid state. *Angew Chem Int Edit* **2002,** *41* (1), 48-76.

65. Maier, J. A.; Martinez, C.; Kasavajhala, K.; Wickstrom, L.; Hauser, K. E.; Simmerling, C., ff14SB: Improving the Accuracy of Protein Side Chain and Backbone Parameters from ff99SB. *J Chem Theory Comput* **2015,** *11* (8), 3696-3713.

66. Wang, J. M.; Wolf, R. M.; Caldwell, J. W.; Kollman, P. A.; Case, D. A., Development and testing of a general amber force field. *J Comput Chem* **2004,** *25* (9), 1157-1174.

67. Bayly, C. I.; Cieplak, P.; Cornell, W. D.; Kollman, P. A., A Well-Behaved Electrostatic Potential Based Method Using Charge Restraints for Deriving Atomic Charges - the Resp Model. *J Phys Chem-Us* **1993,** *97* (40), 10269-10280.

68. Sondergaard, C. R.; Olsson, M. H. M.; Rostkowski, M.; Jensen, J. H., Improved Treatment of Ligands and Coupling Effects in Empirical Calculation and Rationalization of pK(a) Values. *J Chem Theory Comput* **2011,** *7* (7), 2284-2295.

69. Jorgensen, W. L.; Chandrasekhar, J.; Madura, J. D.; Impey, R. W.; Klein, M. L., Comparison of Simple Potential Functions for Simulating Liquid Water. *J Chem Phys* **1983,** *79* (2), 926-935.

70. Izaguirre, J. A.; Catarello, D. P.; Wozniak, J. M.; Skeel, R. D., Langevin stabilization of molecular dynamics. *J Chem Phys* **2001,** *114* (5), 2090-2098.

71. Berendsen, H. J. C.; Postma, J. P. M.; Vangunsteren, W. F.; Dinola, A.; Haak, J. R., Molecular-Dynamics with Coupling to an External Bath. *J Chem Phys* **1984,** *81* (8), 3684-3690.

72. Krautler, V.; Van Gunsteren, W. F.; Hunenberger, P. H., A fast SHAKE: Algorithm to solve distance constraint equations for small molecules in molecular dynamics simulations. *J Comput Chem* **2001,** *22* (5), 501-508.

73. Darden, T.; York, D.; Pedersen, L., Particle Mesh Ewald - an N.Log(N) Method for Ewald Sums in Large Systems. *J Chem Phys* **1993,** *98* (12), 10089-10092.

74. Salomon-Ferrer, R.; Götz, A. W.; Poole, D.; Le Grand, S.; Walker, R. C., Routine Microsecond Molecular Dynamics Simulations with AMBER on GPUs. 2. Explicit Solvent Particle Mesh Ewald. *J Chem Theory Comput* **2013,** *9* (9), 3878-3888.

75. D.A. Case, H. M. A., K. Belfon, I.Y. Ben-Shalom, J.T. Berryman, S.R. Brozell, D.S. Cerutti, T.E.; Cheatham, I., G.A. Cisneros, V.W.D. Cruzeiro, T.A. Darden, N. Forouzesh, M. Ghazimirsaeed, G. Gi amba¸su, T. Giese, M.K. Gilson, H. Gohlke, A.W. Goetz, J. Harris, Z. Huang, S. Izadi, S.A. Izmailov, K.; Kasavajhala, M. C. K., I. Kolossváry, A. Kovalenko, T. Kurtzman, T.S. Lee, P. Li, Z. Li, C. Lin, J. Liu,; T. Luchko, R. L., M. Machado, M. Manathunga, K.M. Merz, Y. Miao, O. Mikhailovskii, G. Monard, H.; Nguyen, K. A. O. H., A. Onufriev, F. Pan, S. Pantano, A. Rahnamoun, D.R. Roe, A. Roitberg, C. Sagui,; S. Schott-Verdugo, A. S., J. Shen, C.L. Simmerling, N.R. Skrynnikov, J. Smith, J. Swails, R.C. Walker,; J. Wang, J. W., X. Wu, Y. Wu, Y. Xiong, Y. Xue, D.M. York, C. Zhao, Q. Zhu, and P.A. Kollman, AMBER 2024. *University of California: San Francisco* **2024**.

76. Swails, J. M.; York, D. M.; Roitberg, A. E., Constant pH Replica Exchange Molecular Dynamics in Explicit Solvent Using Discrete Protonation States: Implementation, Testing, and Validation. *J Chem Theory Comput* **2014,** *10* (3), 1341-1352.

77. Mongan, J.; Case, D. A.; McCammon, J. A., Constant pH molecular dynamics in generalized born implicit solvent. *J Comput Chem* **2004,** *25* (16), 2038-2048.

78. Wang, Z. F.; Fu, X. D.; Diao, W. W.; Wu, Y.; Rovira, C.; Wang, B. J., Theoretical study of the in situ formation of H2O2 by lytic polysaccharide monooxygenases: the reaction mechanism depends on the type of reductant. *Chem Sci* **2025,** *16* (7), 3173-3186.

79. Bakowies, D.; Thiel, W., Hybrid models for combined quantum mechanical and molecular mechanical approaches. *J Phys Chem-Us* **1996,** *100* (25), 10580-10594.

80. Senn, H. M.; Thiel, W., QM/MM Methods for Biomolecular Systems. *Angew Chem Int Edit* **2009,** *48* (7), 1198-1229.

81. Metz, S.; Kästner, J.; Sokol, A. A.; Keal, T. W.; Sherwood, P., ChemShell-a modular software package for QM/MM simulations. *Wires Comput Mol Sci* **2014,** *4* (2), 101-110.

82. Ahlrichs, R.; Bar, M.; Haser, M.; Horn, H.; Kolmel, C., Electronic-Structure Calculations on Workstation Computers - the Program System Turbomole. *Chem Phys Lett* **1989,** *162* (3), 165-169.

83. Smith, W., DL_POLY-applications to molecular simulation II. *Mol Simulat* **2006,** *32* (12-13), 933-933.

84. Lee, C. T.; Yang, W. T.; Parr, R. G., Development of the Colle-Salvetti Correlation-Energy Formula into a Functional of the Electron-Density. *Phys Rev B* **1988,** *37* (2), 785-789.

85. Becke, A. D., Density-Functional Thermochemistry .2. The Effect of the Perdew-Wang Generalized-Gradient Correlation Correction. *J Chem Phys* **1992,** *97* (12), 9173-9177.

86. Becke, A. D., Density-Functional Thermochemistry .3. The Role of Exact Exchange. *J Chem Phys* **1993,** *98* (7), 5648-5652.

87. Nikkel, D. J.; Deak, T. K.; Wetmore, S. D., Insights into the Debated Lyase Mechanism of Bifunctional DNA Glycosylases from MD and QM/MM MD Simulations: The Case Study of DNA Oxidative Damage Repair by Human 8-Oxoguanine DNA Glycosylase. *J Am Chem Soc* **2026,** *148* (22), 23343-23356.

88. Grimme, S., Semiempirical GGA-type density functional constructed with a long-range dispersion correction. *J Comput Chem* **2006,** *27* (15), 1787-1799.

89. Skodje, R. T.; Truhlar, D. G., Parabolic Tunneling Calculations. *J Phys Chem-Us* **1981,** *85* (6), 624-628.

90. Lu, T., TSTcalculator, http://sobereva.com/310.

91. Zhang, Q. Y.; Chen, Q. Q.; Shaik, S.; Wang, B. J., Flavin-N5OOH Functions as both a Powerful Nucleophile and a Base in the Superfamily of Flavoenzymes. *Angew Chem Int Edit* **2024,** *63* (14).

92. Wang, Y. C.; Shaik, S.; Wang, B. J., Heme-Peroxo Intermediate: A Powerful Oxidant in Cytochrome P450 that is Controlled by the Proton Channel of the Protein. *Acs Catal* **2025,** *15* (13), 11277-11292.

93. Zhang, X.; Wang, L. T.; Liu, J.; Chen, T. Y.; Yan, S. H.; Chang, W. C.; Shaik, S.; Zhou, J. H.; Wang, B. J., An Alternative Mechanism for C-C Desaturation Underscores a Dual-Controlled Mechanism for the Fate of Radical Intermediate in Iron(II)- and 2-(Oxo)glutarate-Dependent Oxygenase DfmD. *J Am Chem Soc* **2025,** *147* (24), 20442-20455.

94. Sheng, J. X.; Zhang, X. H.; Liang, Z.; Li, X. W.; Ma, D. X.; Xia, Q. Y.; Liu, Y. J., Catalytic Mechanism of γ-Elimination and Michael Addition Catalyzed by Pyridoxal-5′-Phosphate-Dependent γ-Substitution Enzyme Fub7 Involved in the Biosynthesis of 5-Alkyl-pipecolic Acid. *J Chem Inf Model* **2026**.

95. Zhu, Y. G.; Wang, Y. C.; Zhang, L. P.; Fang, C. Y.; Yong, Y. H.; Chen, R. J.; Zhou, J. H.; Zhang, Q. B.; Wang, B. J.; Zhang, C. S., A Cytochrome P450 Enzyme-Catalyzed Acetyl Migration in Cyanogramide Biosynthesis. *Angew Chem Int Edit* **2026**.

96. Shaik, S.; Cohen, S.; Wang, Y.; Chen, H.; Kumar, D.; Thiel, W., P450 Enzymes: Their Structure, Reactivity, and Selectivity-Modeled by QM/MM Calculations. *Chem Rev* **2010,** *110* (2), 949-1017.

97. Chen, Z. Q.; Zhang, C. H.; Xue, Y., Theoretical Studies on the Thermodynamics and Kinetics of the N-Glycosidic Bond Cleavage in Deoxythymidine Glycol. *J Phys Chem B* **2009,** *113* (30), 10409-10420.

98. Sebera, J.; Hattori, Y.; Sato, D.; Reha, D.; Nencka, R.; Kohno, T.; Kojima, C.; Tanaka, Y.; Sychrovsky, V., The mechanism of the glycosylase reaction with hOGG1 base-excision repair enzyme: concerted effect of Lys249 and Asp268 during excision of 8-oxoguanine. *Nucleic Acids Res* **2017,** *45* (9), 5231-5242.

99. Lenz, S. A. P.; Wetmore, S. D., QM/MM Study of the Reaction Catalyzed by Alkyladenine DNA Glycosylase: Examination of the Substrate Specificity of a DNA Repair Enzyme. *J Phys Chem B* **2017,** *121* (49), 11096-11108.

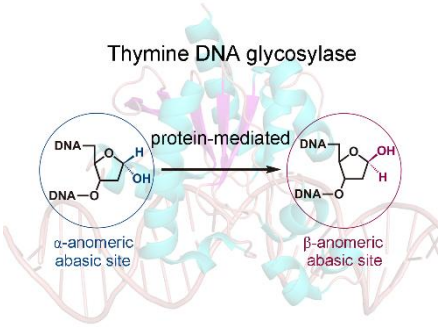
100. Zhao, Y.; Truhlar, D. G., The M06 suite of density functionals for main group thermochemistry, thermochemical kinetics, noncovalent interactions, excited states, and transition elements: two new functionals and systematic testing of four M06-class functionals and 12 other functionals. *Theor Chem Acc* **2008,** *120* (1-3), 215-241.

101. Marenich, A. V.; Cramer, C. J.; Truhlar, D. G., Universal Solvation Model Based on Solute Electron Density and on a Continuum Model of the Solvent Defined by the Bulk Dielectric Constant and Atomic Surface Tensions. *J Phys Chem B* **2009,** *113* (18), 6378-6396.

102. Frisch, M. J.; Trucks, G. W.; Schlegel, H. B.; Scuseria, G. E.; Robb, M. A.; Cheeseman, J. R.; Scalmani, G.; Barone, V.; Petersson, G. A.; Nakatsuji, H.; Li, X.; Caricato, M.; Marenich, A. V.; Bloino, J.; Janesko, B. G.; Gomperts, R.; Mennucci, B.; Hratchian, H. P.; Ortiz, J. V.; Izmaylov, A. F.; Sonnenberg, J. L.; Williams-Young, D.; Ding, F.; Lipparini, F.; Egidi, F.; Goings, J.; Peng, B.; Petrone, A.; Henderson, T.; Ranasinghe, D.; Zakrzewski, V. G.; Gao, J.; Rega, N.; Zheng, G.; Liang, W.; Hada, M.; Ehara, M.; Toyota, K.; Fukuda, R.; Hasegawa,

J.; Ishida, M.; Nakajima, T.; Honda, Y.; Kitao, O.; Nakai, H.; Vreven, T.; Throssell, K.; Montgomery, J. A.; Peralta, J. A.; Ogliaro, F.; Bearpark, M. J.; Heyd, J. J.; Brothers, E. N.; K. N. Kudin; V. N. Staroverov; T. A. Keith; R. Kobayashi; J. Normand; K. Raghavachari; A. P. Rendell; J. C. Burant; S. S. Iyengar; J. Tomasi; M. Cossi; J. M. Millam; M. Klene; C. Adamo; R. Cammi; J. W. Ochterski; R. L. Martin; K. Morokuma; O. Farkas; J. B. Foresman; Fox, D. J., Gaussian 16, Revision A.03. Wallingford CT, 2016.

Table of Contents



Supplementary Files

This is a list of supplementary files associated with this preprint. Click to download.

- SI1028Double.pdf